NASA/TM—2012-215982

Design and Analysis of an Isokinetic Sampling Probe for Submicron Particle Measurements at High Altitude

Christopher M. Heath
Glenn Research Center, Cleveland, Ohio

February 2012

NASA STI Program . . . in Profile

Since its founding, NASA has been dedicated to the advancement of aeronautics and space science. The NASA Scientific and Technical Information (STI) program plays a key part in helping NASA maintain this important role.

The NASA STI Program operates under the auspices of the Agency Chief Information Officer. It collects, organizes, provides for archiving, and disseminates NASA's STI. The NASA STI program provides access to the NASA Aeronautics and Space Database and its public interface, the NASA Technical Reports Server, thus providing one of the largest collections of aeronautical and space science STI in the world. Results are published in both non-NASA channels and by NASA in the NASA STI Report Series, which includes the following report types:

- TECHNICAL PUBLICATION. Reports of completed research or a major significant phase of research that present the results of NASA programs and include extensive data or theoretical analysis. Includes compilations of significant scientific and technical data and information deemed to be of continuing reference value. NASA counterpart of peer-reviewed formal professional papers but has less stringent limitations on manuscript length and extent of graphic presentations.

- TECHNICAL MEMORANDUM. Scientific and technical findings that are preliminary or of specialized interest, e.g., quick release reports, working papers, and bibliographies that contain minimal annotation. Does not contain extensive analysis.

- CONTRACTOR REPORT. Scientific and technical findings by NASA-sponsored contractors and grantees.

- CONFERENCE PUBLICATION. Collected papers from scientific and technical conferences, symposia, seminars, or other meetings sponsored or cosponsored by NASA.

- SPECIAL PUBLICATION. Scientific, technical, or historical information from NASA programs, projects, and missions, often concerned with subjects having substantial public interest.

- TECHNICAL TRANSLATION. English-language translations of foreign scientific and technical material pertinent to NASA's mission.

Specialized services also include creating custom thesauri, building customized databases, organizing and publishing research results.

For more information about the NASA STI program, see the following:

- Access the NASA STI program home page at *http://www.sti.nasa.gov*

- E-mail your question via the Internet to *help@sti.nasa.gov*

- Fax your question to the NASA STI Help Desk at 443–757–5803

- Telephone the NASA STI Help Desk at 443–757–5802

- Write to:
  NASA Center for AeroSpace Information (CASI)
  7115 Standard Drive
  Hanover, MD 21076–1320

NASA/TM—2012-215982

Design and Analysis of an Isokinetic Sampling Probe for Submicron Particle Measurements at High Altitude

Christopher M. Heath
Glenn Research Center, Cleveland, Ohio

National Aeronautics and
Space Administration

Glenn Research Center
Cleveland, Ohio 44135

February 2012

This report is a formal draft or working paper, intended to solicit comments and ideas from a technical peer group.

This report contains preliminary findings, subject to revision as analysis proceeds.

This work was sponsored by the Fundamental Aeronautics Program at the NASA Glenn Research Center.

Level of Review: This material has been technically reviewed by technical management.

Available from

NASA Center for Aerospace Information
7115 Standard Drive
Hanover, MD 21076–1320

National Technical Information Service
5301 Shawnee Road
Alexandria, VA 22312

Available electronically at http://www.sti.nasa.gov

Design and Analysis of an Isokinetic Sampling Probe for Submicron Particle Measurements at High Altitude

Christopher M. Heath
National Aeronautics and Space Administration
Glenn Research Center
Cleveland, Ohio 44135

Abstract

An isokinetic tip dilution probe has been designed with the aid of computational fluid dynamics to sample sub-micron particles emitted from aviation combustion sources. The intended operational range includes standard day atmospheric conditions up to 40,000-ft. With dry nitrogen as the diluent, the probe is intended to minimize losses from particle microphysics and transport while rapidly quenching chemical kinetics. Initial results indicate that the Mach number ratio of the aerosol sample and dilution streams in the mixing region is an important factor for successful operation. Flow rate through the probe tip was found to be highly sensitive to the static pressure at the probe exit. Particle losses through the system were estimated to be on the order of 50 percent with minimal change in the overall particle size distribution apparent. Particle size distributions and number densities from various combustion sources will be used to better understand particle-phase microphysics, plume chemistry, evolution to cirrus, and environmental impacts of aviation.

Nomenclature

Symbols:

d_0	Source diameter (i.e., Nozzle exit diameter = 1.27-cm)
d^*	Far field equivalent source diameter
D_{ratio}	Ratio of dilution to sample by mass
$P_{0,\infty}$	Total chamber pressure far from nozzle exit
$T_{0,\infty}$	Total chamber temperature far from nozzle exit
$\rho_{0,\infty}$	Total chamber pressure density far from nozzle exit
U_x	Axial velocity x distance from the nozzle exit
$P_{0,x}$	Total pressure x distance from nozzle exit
$T_{0,x}$	Total temperature x distance from nozzle exit
$\rho_{0,x}$	Total density x distance from nozzle exit
$R_{0,x}$	Specific gas constant distance x from nozzle exit
$P_{0,Nozzle}$	Total pressure at burner exit
$T_{0,Nozzle}$	Total temperature at burner exit
$\rho_{0,Nozzle}$	Total density at burner exit
P_S	Static pressure
T_S	Static temperature
$\dot{m}_{Nozzle}$	Mass flow rate of burner exhaust products
U_∞	Axial velocity of chamber co-flow
x	Axial distance from nozzle exit
x_E	Axial distance from virtual origin to jet exit plane

Abbreviations:

CFD	Computational Fluid Dynamics
CPC	Condensation Particle Counter
EC	Electrostatic Classifier
FAR	Fuel-to-Air Ratio
GCM	Global Circulation Model
NCC	National Combustion Code
NASA	National Aeronautics and Space Administration
PAL	Particle Aerosol Laboratory
SGAPE	Streamline-based Gas and Particle Emission
SMPS	Scanning Mobility Particle Sizer
N_2	Diatomic nitrogen

Introduction

Quantifying the impact of civil aviation emissions on global climate change, local air quality and human health has become a growing difficulty for many regulating agencies. General Circulation Models (GCMs) have become the primary tool for estimating long-term effects of increasing air traffic on climate. Despite efforts, the magnitude and sign of radiative forcing resultant solely from aviation remains elusive to the general scientific community. To aid understanding, an improved and comprehensive inventory of the current global aerosol background is needed. This data, combined with controlled experimental measurements of emission/atmosphere interactions, will offer a step forward in understanding how complex particle and gas-phase interactions influence the environment.

To gain a better grasp on the microphysical and chemical mechanisms that allow contrails from aviation to form cirrus, in-situ measurements at well-controlled atmospheric conditions will play a key role. The Particle Aerosol Laboratory (PAL) at the NASA Glenn Research Center was established to provide just this capability. The facility consists of a flow through altitude chamber that simulates standard day atmosphere conditions up to 40,000 ft. Background chamber temperature, pressure and relative humidity are all variable parameters. Exhaust from a combustor capable of burning jet fuel is injected through a nozzle directly into the altitude chamber. Variable burner settings include fuel composition, equivalence ratio, combustor temperature and pressure. Volatile and non-volatile particulate matter (PM) may be extracted directly from the burner or chamber via a probe and sampling line. Inside the chamber, the probe can be positioned at several axial and radial distances from the exhaust injection site. Particle output from the combustor, in terms of number density and size distributions, are used to study contrail formation and early evolution.

Plume characterization is typically performed using a standard Scanning Mobility Particle Sizer (SMPS) spectrometer, (TSI, Inc. Model 3936NL76), retrofitted to operate at low pressure. The SMPS suite consists of a TSI model 3080 Electrostatic Classifier (EC) and a 3776 Condensation Particle Counter (CPC) connected in series. More in-depth information in terms of plume chemistry and particle morphology may be acquired by applying non-intrusive methods in concert with additional extractive sampling techniques.

In the past, quantitative particle measurements using standard sampling probes have proven problematic at simulated high altitude conditions. Difficulties with extractive measurements have included (1) ice accretion on the probe inlet where relative humidity exceeds 100 percent,(2) non-axial flow at the probe inlet resulting in flow separation, turbulence and particle deposition, (3) particle transport losses due to electrostatic effects, diffusion, inertial forces, thermophoresis and coagulation, and (4) extractive sampling at relatively low pressure near 0.2-atm. Problem (1) is common when sampling within short distances from the combustor exit plane due to the high water vapor present in the aircraft

exhaust which condenses rapidly and freezes to the probe inlet at cold temperatures. To date, heated probes have been tested in the altitude chamber but with limited success (Ref. 1). The higher probe wall temperature has been found to cause vaporization of the volatile particle fraction, producing a change in the total particle size distribution and overall number concentration measured. Particle output becomes a function of probe wall temperature, making measurements difficult to quantify. For the probe designed here, neither the effect of ice accretion nor elevated probe wall temperatures were modeled. Problems 2 through 4 were addressed more directly during the design process.

Altitude Chamber Facility

The Particle Aerosol Laboratory (PAL) at the NASA Glenn Research Center consists of a low pressure burner whose output is connected to a flow-through altitude simulation chamber. The burner, comprised of a combustion chamber and downstream mixing section, typically operates between 1 to 2-atm and burns traditional aviation fuel. Alternative and bio-fuel blends such as Fischer Tropsch may also be used. The altitude chamber can match atmospheric conditions (temperature and pressure) up to 40,000-ft. Background relative humidity can also be varied up to 100 percent for lower altitude operation. Maximum relative humidity at higher altitudes (above 35,000-ft) is reduced due to facility limitations. A cold nitrogen supply offers the working fluid for the chamber. Combustion byproducts are injected upward from the base of the chamber through an insulated transition pipe measuring 2.43-cm in diameter by 1.6-m in length. The transition pipe terminates at a 1.27-cm diameter nozzle. A vertical instrumentation plate is located on one side of the chamber and contains several 1/4-in. ports at discrete axial distances from the nozzle exit. A sampling probe may be inserted through any port and used to extract exhaust products for characterization. Three double paned windows are positioned around the remaining circumference of the chamber and provide limited optical access. The N_2 co-flow and combustion products exit the altitude chamber through an exhaust duct located on top. Figure 1 is a diagram of the altitude simulation chamber and low pressure burner. More details on the burner and chamber operation, including chamber background temperature and pressure profiles, are provided in Reference 1.

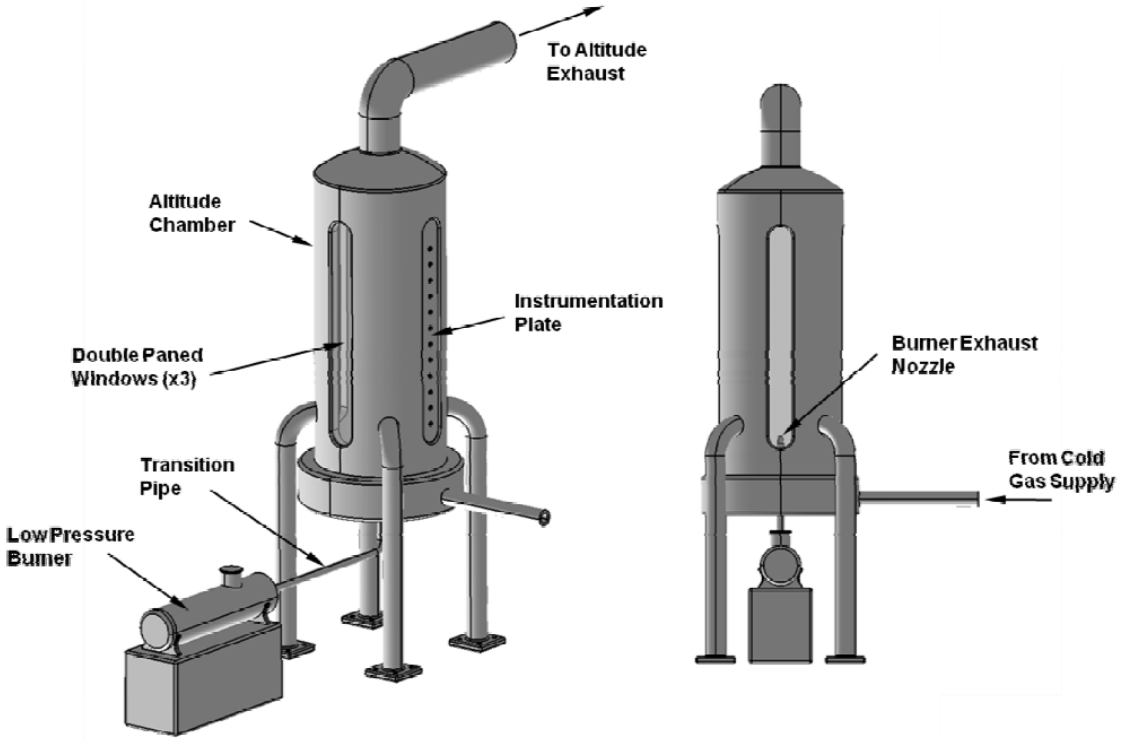

Figure 1.—Particle Aerosol Laboratory (PAL) comprised of an altitude chamber and low-pressure combustor.

On-Design Specifications

An aerosol sampling probe, consisting of an inner sampling line enclosed by a coaxial outer hull through which dilution flows, has been designed to extract plume samples from a low pressure, low velocity environment. The probe contains a shallow 90° bend so that it can be inserted through any port on the side of the altitude chamber and point downward directly into the primary flow. Figure 2(a) shows an orthogonal view of the complete dilution probe as well as a full-section view of the probe entrance. Both the inner sampling line and outer dilution housing have circular cross-sections. The probe region analyzed in this study was the sample inlet and mixing section up to 5.14E-2-m from the probe tip, shown in Figure 2(b). The 90° bend, aft probe section, and sampling line to the instruments were not considered. Typical operation was expected to be near 40,000-ft standard day conditions, which has proven highly problematic in previous experiments due to a number of complications (Refs. 1 to 2). Table 1 lists the chamber background conditions from which the probe was designed to operate.

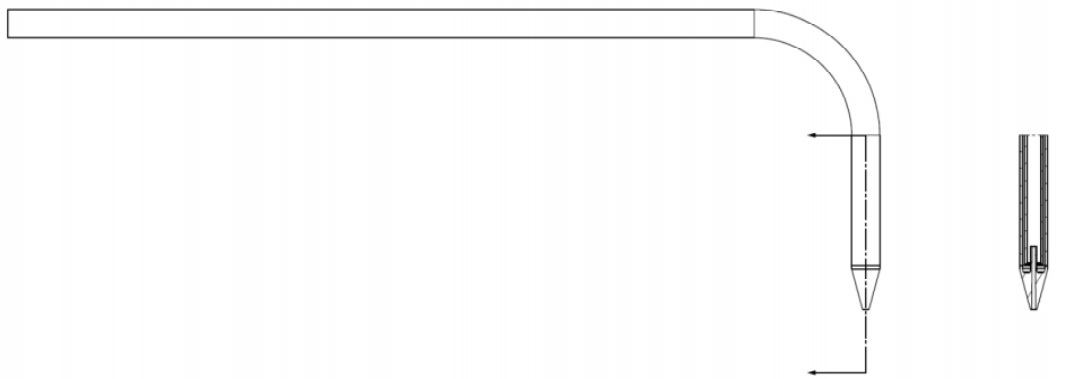

Figure 2(a).—External view of aerosol sampling probe with full-section view of the sample/dilution mixing region.

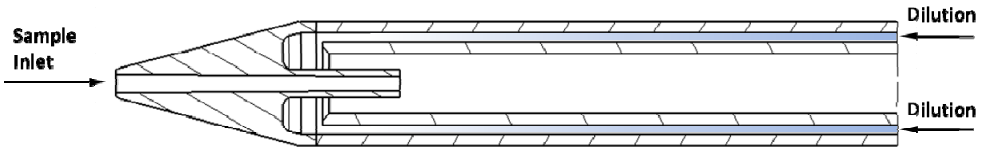

Figure 2(b).—Definition of sample and dilution flow paths.

TABLE 1.—BACKGROUND ALTITUDE CONDITIONS FOR SAMPLING DESIGN POINT

Altitude Chamber Conditions (40,000-ft)		
U_∞	0.0	m/s
$\rho_{s,\infty}$ @ 40,000-ft std. day	0.3016	kg/m^3
$P_{s,\infty}$ @ 40,000-ft std. day	18.753	kPa
$T_{s,\infty}$ @ 40,000-ft std. day	216.65	K

TABLE 2.—BURNER EXHAUST CONDITIONS FOR SAMPLING DESIGN POINT

Burner Exhaust Conditions		
d_0	1.27E-2	m
FAR	0.045	-
$\dot{m}_{Nozzle}$	2.76E-3	kg/s
$T_{s,Nozzle}$	540	K
$P_{s,Nozzle}$	18.753	kPa
$\rho_{s,Nozzle}$	0.121	kg/m^3

Burner conditions were set based on previous experimental measurements. Exhaust specifications at the exit of the burner are listed in Table 2, where d_0 is the physical diameter of the nozzle exit through which exhaust products enter the chamber.

The distance from the nozzle exit to the probe tip, denoted *x*, was defined as 0.71-m for the on-design sampling condition. Previous measurements show the chamber flow is momentum-dominated in this region, meaning buoyancy effects may be considered negligible (Ref. 1). Using the nozzle exit and background chamber conditions, momentum-dominated jet scaling laws were applied to approximate temperature, pressure and density along the jet centerline where sampling will occur. Static pressure at the nozzle exit was assumed to equal that of the chamber ($P_{s,x} \approx P_{s,\infty}$). The chamber coflow velocity was near 0.7-m/s and assumed negligible ($U_\infty \approx 0$) compared to the average velocity of the jet. Exhaust products exiting the nozzle were assumed to exhibit a top-hat profile.

For a non-reacting turbulent jet issuing from a nozzle, the finite-area source (i.e., nozzle exit area) may be approximated by an equivalent ideal point source located upstream of the nozzle exit plane. The location of the ideal point source is referred to as the virtual origin, making x_E the axial distance between the virtual origin and the nozzle exit plane. For momentum-dominated jets, self similarity scaling has shown that a conserved scalar (i.e., normalized temperature difference) is inversely proportional to the normalized distance from the virtual origin (Ref. 3).

For example,

$$\frac{T_{s,x} - T_{s,\infty}}{T_{S,\ \mathrm{Nozzle}} - T_{s,\infty}} = 5.4\left(\frac{x + x_E}{d^*}\right)^{-1} \tag{1}$$

where x_E may be approximated by Equation (2). For the on-design conditions in Tables 1 and 2, x_E has been calculated previously to be 0.28-m (Ref. 1). For jets issuing with a uniform velocity profile, constant density and from a circular nozzle, d^* is the far-field equivalent source diameter given by Equation (3). d^* was first proposed to account for the density differences between an axisymmetric turbulent jet and the surrounding ambient fluid assuming no heat release occurs (Ref. 3).

$$x_E \approx 3.6\, d^* \tag{2}$$

$$d^* = d_0 \sqrt{\frac{\rho_{s,\infty}}{\rho_{s,\mathrm{Nozzle}}}} = d_0 \sqrt{\frac{T_{S,\infty}}{T_{S,\mathrm{Nozzle}}}} \tag{3}$$

Rearranging (1) provides a solution for the jet centerline temperature at distance *x* downstream of the nozzle exit.

$$T_{S,x} = \frac{c_\theta \left(T_{S,\,\text{Burner}} - T_{S,\infty} \right) d^*}{\left(x + x_E \right)} + T_{S,\infty} \tag{4}$$

The axial velocity along a jet centerline may be calculated by applying Equation (5), as given in Reference 4.

$$U_x = 6.5 \left(U_0 \frac{d^*}{x} \right) \tag{5}$$

The density along the jet centerline at downstream distance x from the nozzle exit may be calculated by applying the ideal gas law and assuming the specific gas constant in the jet equals that of the chamber background ($R_x \approx R_\infty$). This assumption is typically within the accuracy of the self-similar jet scaling laws applied.

$$\rho_{s,x} = \frac{P_{S,x}}{R_x T_{s,x}} \tag{6}$$

On-design sampling conditions in the plume, as determined from Equations (1) to (6), are listed in Table 3.

TABLE 3.—PROBE INLET CONDITIONS FOR SAMPLING DESIGN POINT

Sampling Probe Inlet Conditions (40,000-ft)		
x	0.71	m
x_E	0.028	m
d^*	8.044E-3	m
U_x	13.288	m/s
$T_{s,x}$	235.77	K
$P_{s,x}$	18.753	kPa
$\rho_{s,x}$	0.277	kg/m^3

Based on prior analysis of high dilution sampling probes for ground-level emission measurements, a dilution ratio near 20:1 was selected for standard operation. High dilution using an inert gas is known to rapidly quench chemistry that tends to occur as a sample is drawn through a probe and/or transport line.

Parametric Sampling Probe Geometry

A three-dimensional parametric model for a high dilution sample probe was developed in CATIA V5 R20. Figure 3 defines the standard geometry. Design parameters include the inner diameter of the sample inlet, inner diameter of the sample exit, and outer diameter of the sample exit. Changing the sample inlet and sample exit inner diameters for any given design allows the sample flow to be accelerated, decelerated, or held constant. Figure 3 shows a design in which the sample inlet flow is accelerated.

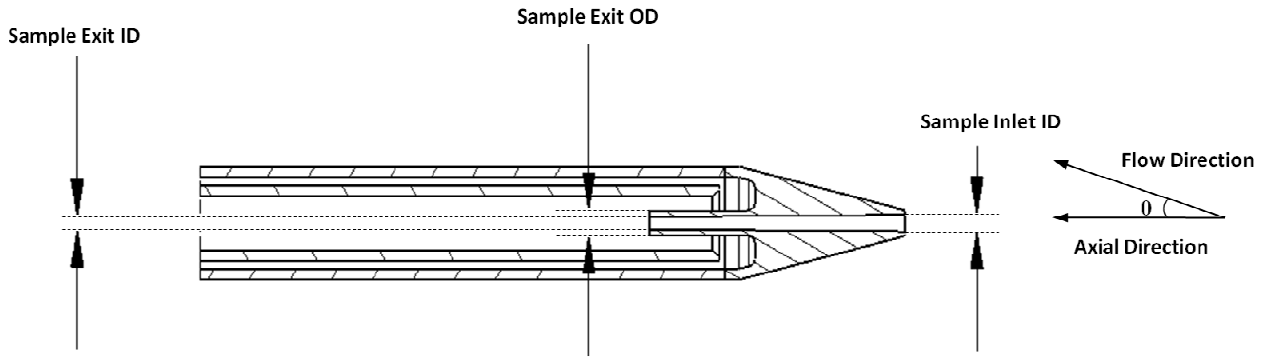

Figure 3.—Description of variable geometric parameters for the high dilution sampling probe design.

Design Problem Formulation

The sampling probe was designed to ensure incoming flow streamlines remained isokinetic, flow through the probe remained steady and absent of strong turbulent eddies, and the shape of a given particle size distribution did not change significantly throughout the probe.

Design Objectives

$$\text{Average flow upstream of sample inlet } \theta < 0.5° \text{ from axial direction} \tag{7}$$

$$\text{Mixing region absent of turbulent eddies} \tag{8}$$

$$\text{Shape of particle size distribution at sample inlet remains consistent at probe exit} \tag{9}$$

To keep designs practical in terms of cost and manufacturability, the internal and external tube diameters were forced to be consistent with standard stainless steel tube dimensions. The internal sampling tube was assumed to have a 1/4-in. outer diameter with 0.035-in. wall thickness. The outer probe housing confining the dilution flow was assumed to have a 0.375-in. outer diameter with 0.035-in. wall thickness. By setting both tube diameters, the only custom feature of the sampling probe became the tip, which was designed to interface directly with the standard stainless steel tube sizes.

The following physical constraints were placed on the probe tip parameters to eliminate the potential for impossible or difficult to manufacture geometries:

$$\text{Sample Exit Outer Diameter} < 0.305\text{-in.} \tag{10}$$

$$\text{Sample Exit Outer Diameter} - \text{Sample Exit Inner Diameter} > 0.04\text{-in.} \tag{11}$$

$$\text{Sample Inlet Inner Diameter} > 0.025\text{-in.} \tag{12}$$

$$\text{Sample Exit Inner Diameter} > 0.025\text{-in.} \tag{13}$$

Equation (10) ensures that the outer diameter of the sample exit is less than the fixed inner diameter of the internal sampling tube. Equations (11) to (13) ensure manufacturability and material strength are maintained.

First-Order Modeling

A single point design strategy was applied by combining a first-order mixer model developed using the Numerical Propulsion System Simulation (NPSS) with a Computational Fluid Dynamics (CFD) code. The National Combustion Code (NCC) served as the flow solver. The probe was modeled in NPSS using six separate flow elements. Figure 4 contains a block diagram of the NPSS model with description of inputs and outputs for each flow station. Model outputs were used to predict probe geometry and flow station boundary conditions assuming ideal one-dimensional mixing.

The NPSS model contains two independent flow streams: a sample inlet flow extracted from the plume centerline (Station 1) and a higher pressure and temperature dilution flow (Station 3). A two percent pressure loss was assumed between Stations 1 and 2 due to viscous effects. Upon exiting the sample region (Station 2), the sample flow is mixed with a dilution stream (Station 4) assuming ideal isentropic mixing. The NPSS mixer element assumes that the exit flow area of the mixer is equal to the sum of the flow areas of the two mixing streams. During mixing, the flow simultaneously undergoes an expansion due to the absence of the wall which initially divides Stations 2 and 3. This was modeled by applying a diffuser after the mixer which expands the fluid to match the physical probe exit area (Station 5). Because the expansion occurs almost instantaneously, no pressure drop was assumed in the diffuser element. Output values from Station 5 were used to predict probe exit boundary conditions (Station 6).

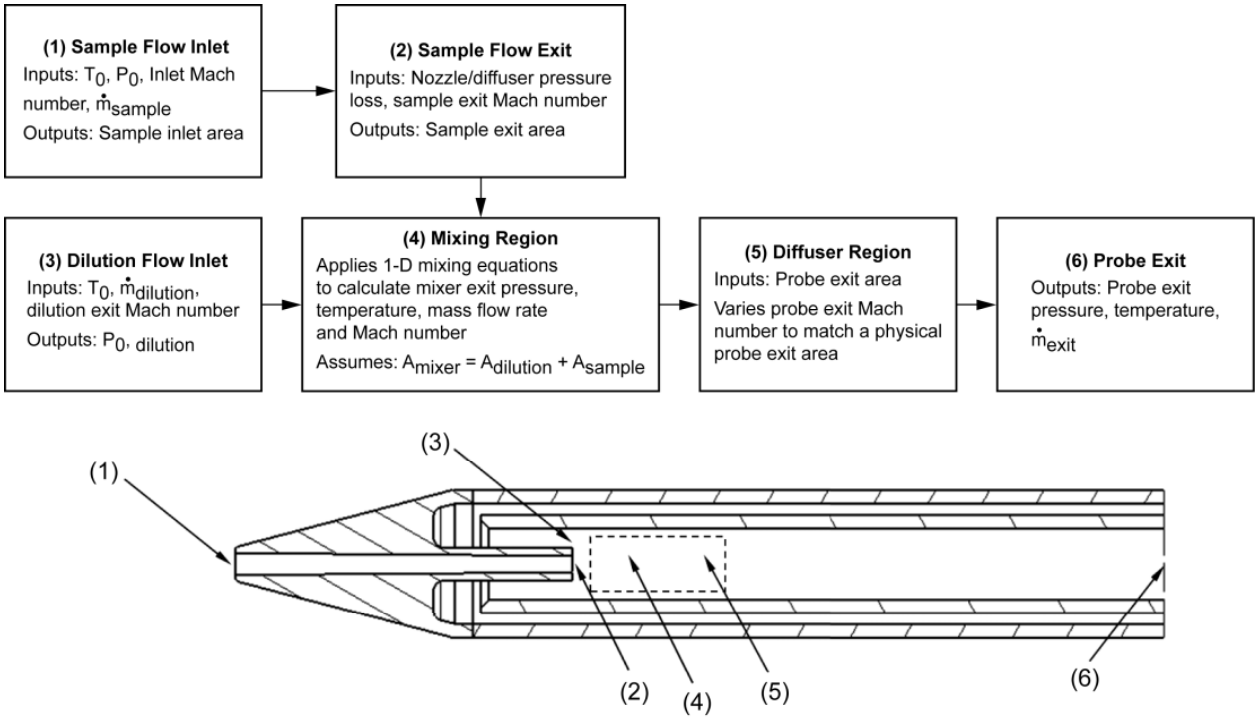

Figure 4.—First-order NPSS model of the high dilution aerosol sampling probe for on-design operation.

Exploration of the design space using the NPSS model produced a large number of feasible designs, many of which exhibited non-ideal mixing characteristics when analyzed with CFD. Performance was found to be sensitive to the Mach number ratio between the two mixing stream and to the back pressure on the probe exit. A significant difference in the two Mach numbers was found to produce a stagnation region just downstream of the sample exit location. This in turn would be accompanied by an internal pressure loss, causing the probe exit pressure boundary condition (estimated from NPSS) to be higher than necessary. A high pressure boundary condition applied at the probe exit tends to produce an expansion upstream of the probe tip, further diluting the incoming sample stream. This type of operation could cause a large discrepancy between the number density of an incoming sample measured and the actual number density of a sample just upstream of the probe tip. Through trial and error, a ratio of sample to dilution Mach numbers around 0.4 was found to produce acceptable internal flow dynamics and mixing.

By adjusting the probe geometric parameters and Mach number ratio between the sample and dilution flows, the design in Table 4 was identified and found to have acceptable on-design performance when analyzed using the National Combustion Code (NCC). Note, the geometric probe parameters are specified in English units to be consistent with standard stainless steel tube dimensions.

TABLE 4.—SAMPLING PROBE DESIGN FROM NPSS MODEL

Probe Geometric Variables		
Sample Inlet Inner Diameter	5.52E-2	in
Sample Exit Inner Diameter	4.14E-2	in
Sample Exit Outer Diameter	8.38E-2	in
Sample Inlet Flow Station		
Sample Inlet P_s	18.753	kPa
Sample Inlet T_s	235.68	K
Sample Inlet Mach Number	0.044	-
Sample Inlet Mass Flow Rate	5.80E-6	kg/s
Sample Exit Flow Station		
Sample Exit P_s	18.296	kPa
Sample Exit T_s	235.378	K
Sample Exit Mach Number	0.080	-
Dilution Exit Flow Station		
Dilution Exit P_s	18.296	kPa
Dilution Exit T_s	293.14	K
Dilution Exit Mach Number	0.121	-
Dilution Exit Mass Flow Rate	1.16E-4	kg/s
Mixer Exit Flow Station		
Mixer Exit P_s	18.298	kPa
Mixer Exit T_s	290.41	K
Mixer Exit Mach Number	0.118	-
Probe Exit Flow Station		
Probe Exit P_s	18.352	kPa
Probe Exit T_s	291.23	K
Probe Exit Mach Number	0.099	-

Computational Fluid Dynamics Modeling

Numerical Methods

A steady-state, non-reacting computation was performed to analyze design point operation using the National Combustion Code (NCC) (Refs. 5 and 6). The NCC uses a cell-centered finite-volume spatial discretization for unstructured grids along with pseudo-time preconditioning. An explicit four-stage Runge-Kutta scheme was applied to advance the solution in pseudo time. Local pseudo-time stepping and residual smoothing were applied to accelerate the convergence. Turbulence was modeled by applying a high Reynolds number k-ε model (Ref. 7). NCC was compiled to use the MPI message passing libraries to leverage the parallel processing capabilities of the code. All computations were executed on a single remote compute node containing 48 AMD Magny-cours processing cores operating at 2.2 GHz. Simulations were set to terminate after a global mass imbalance of 1E-4, determined by Equation (14), had been achieved for 5,000 successive iterations.

$$\text{Mass Imbalance} = \frac{\text{Mass In} - \text{Mass Out}}{\text{Mass In}} \tag{14}$$

Mesh Definition

Calculated flow station parameters from the NPSS model were used to define the probe geometry and initialize the boundary conditions for performing CFD. To reduce computational expense, the probe flow domain was modeled as a three-dimensional 10° sector. An unstructured hexahedral mesh consisting of around 250,000 grid points was applied to the flow domain. The complete mesh is shown in Figure 5(a). Cell density just upstream of the probe tip and inside the probe was increased to resolve boundary layer effects (see Fig. 5(b)). Figure 6 shows boundary conditions applied to each external surface of the domain. The face upstream of the probe was modeled as a flow inlet where a normal velocity component was applied and assumed equal to the free stream jet velocity at 0.71-m downstream of the nozzle exit. Both angled sides of the domain were tagged as symmetry boundaries through which no fluid could enter or exit. The top face was tagged as a flow exit in which the ambient static pressure predicted in the chamber from self similar jet scaling laws was applied. The same condition was used for the adjacent vertical surface downstream of the primary flow inlet. The dilution channel entrance face was tagged as a mass flow inlet in which the flow rate was set to 20 times that of the incoming sample flow rate predicted by the NPSS model. Note, the prescribed dilution mass flow rate in Figure 6 is $1/36^{th}$ that of the value in Table 4 because the flow domain is a 10° sector. The downstream probe exit face was tagged as a flow exit and the static pressure NPSS predicted at that flow station was prescribed.

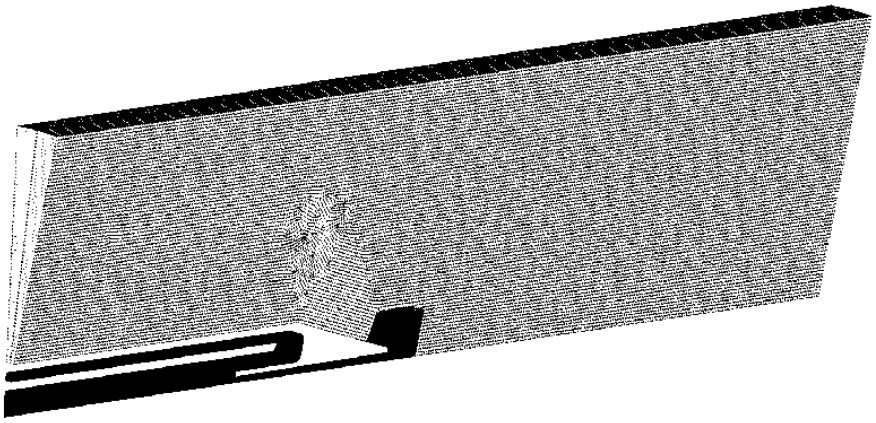

Figure 5(a).—Unstructured hexahedral mesh of the probe flow domain consisting of ~250,000 grid points.

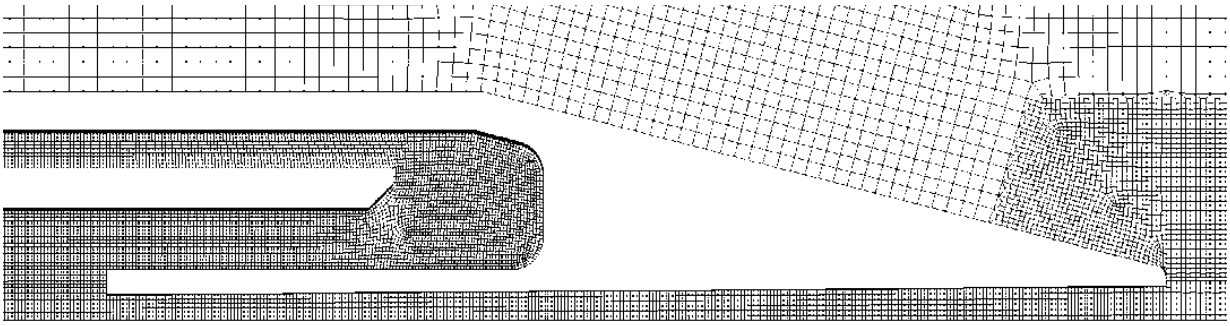

Figure 5(b).—View of refined mesh near the probe inlet and mixing region.

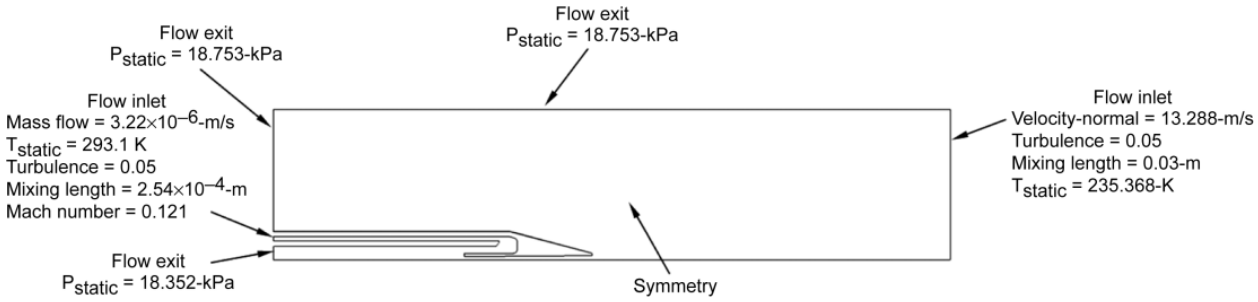

Figure 6.—Definition of boundary conditions applied to the computational flow domain.

Computational Fluid Dynamics Results

Figures 7 to 10 display CFD results for the on-design sampling condition. Streamlines have been added to each contour to indicate axial and radial flow directions. Almost no flow was found to exist in the azimuthal direction. From the streamlines, only minor variation in the flow direction upstream of the probe tip is evident. The probe was found to be streamlined and not cause significant disruption to the incoming fluid. On average, the upstream flow diverges from the axial direction by 0.17°, meaning all fluid entering the probe tip remains isokinetic. The local Mach numbers shown in Figure 7 indicate all flow remains subsonic through the entire domain. Flow field results for the mixing fraction (Fig. 10) indicate the sample and dilution inlet streams mix rapidly and within a short distance from the probe entrance. By the end of the flow domain, both streams appear to be well-mixed. Total residence time through the domain modeled is relatively short and on the order of 0.25-ms.

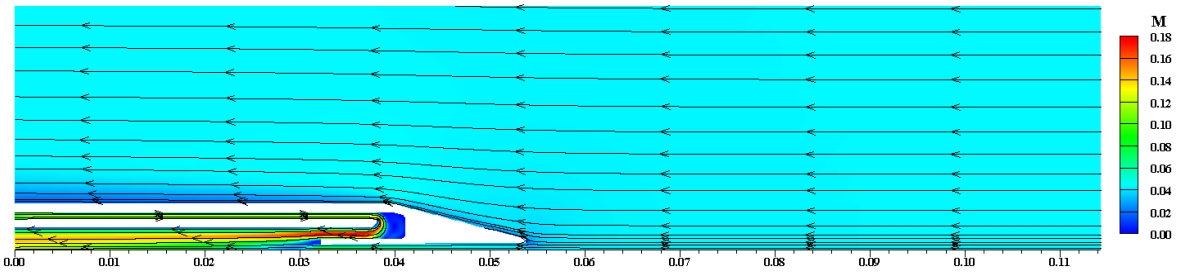

Figure 7.—Vertical plane showing in contour the flow Mach number through the probe inlet.

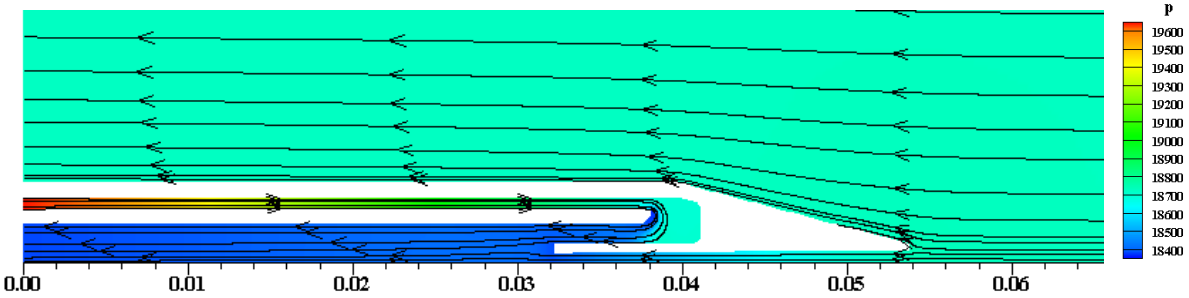

Figure 8.—Vertical plane showing in contour the static pressure through the probe inlet.

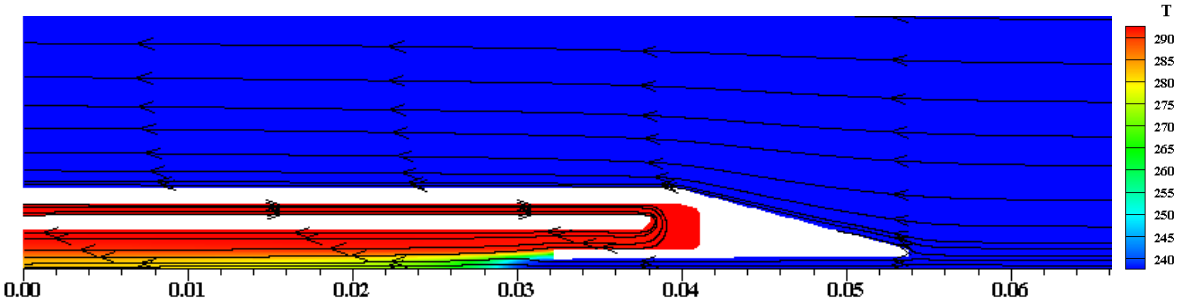

Figure 9.—Vertical plane showing in contour the static temperature through the probe inlet.

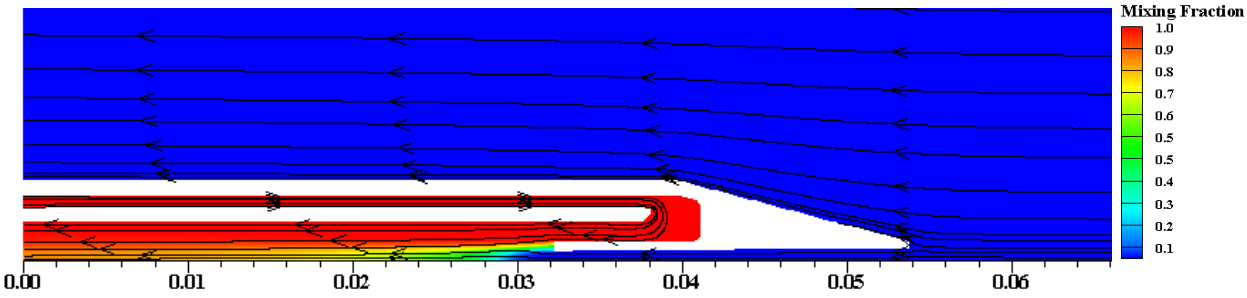

Figure 10.—Vertical plane showing in contour the ratio of dilution to sample flow.

TABLE 5.—SAMPLING PROBE FLOW STATION PARAMETERS FROM CFD

Sample Inlet Flow Station		
Sample Inlet P_s	18.753	kPa
Sample Inlet T_s	235.8	K
Sample Inlet Mach Number	0.034	-
Sample Inlet Mass Flow Rate	4.47E-6	kg/s
Sample Exit Flow Station		
Sample Exit P_s	18.381	kPa
Sample Exit T_s	235.4	K
Sample Exit Mach Number	0.061	-
Dilution Exit Flow Station		
Dilution Exit P_s	18.393	kPa
Dilution Exit T_s	292.5	K
Dilution Exit Mach Number	0.120	-
Dilution Exit Mass Flow Rate	1.16E-4	kg/s
Probe Exit Flow Station		
Probe Exit P_s	18.354	kPa
Probe Exit T_s	291.0	K
Probe Exit Mach Number	0.098	-

Flow station parameters calculated by NCC are provided in Table 5 and were found to be typically within 25 percent of the predicted values from the NPSS solution. Reasons for the difference may be attributed to assumptions regarding ideal mixing in the NPSS model and incorrect pressure loss estimates for the sample inlet. The NPSS model did not account for boundary layer effects, or other general loss mechanisms, but it does provide a place to represent such effects based on the CFD results. The most significant difference between the NPSS model and CFD solution is the sample inlet mass flow rate. The NPSS model appeared to over-predict the probe exit pressure required to keep the sample inlet velocity equal to the free stream velocity of the jet. This caused the sample mass flow rate in NPSS to be nearly 23 percent higher than that predicted by CFD. This discrepancy led to an increase in the dilution-to-sample ratio, D_{ratio}, from 20:1 in NPSS to nearly 26:1 in the CFD solution. Tuning of the low-order model flow station parameters based on CFD results would allow more accurate predictions to be made by NPSS. This may prove useful for future variations on the design. Despite this difference in D_{ratio} from the intended design, the internal flow field and mixing characteristics remain acceptable.

Streamline-Based Particle Modeling

The Streamline-based Gas and Particle Emissions (SGAPE) model was applied to analyze trace chemistry and microphysics occurring inside the sampling probe. SGAPE is a particle deposition and evolution code containing many of the same chemical and microphysical solvers as NCC. To reduce computational expense of a complete reacting CFD model, the software relies on reduced profile information post-processed from a non-reacting CFD flow field. For this work, average velocity, pressure and temperature were extracted along the flow direction from the three-dimensional NCC solution and used as input to the SGAPE code. A finite rate kinetic mechanism involving 29 species and 73 reaction steps was used to model combustion exhaust and atmospheric chemistry interactions. Details on the species and particle transport models used in SGAPE are provided in References 8 and 9. Microphysics considered included soot coagulation, soot activation, condensates forming on soot, scavenging between soot and $H_2SO_4 – H_2O$ droplets, $H_2SO_4 – H_2O$ nucleation, $H_2SO_4 – H_2O$ coagulation, and condensation on $H_2SO_4 – H_2O$ droplets.

Exhaust Composition

Prescribed sample inlet exhaust conditions were assumed to represent a worst-case scenario for general aviation fuel. This means that an unexpectedly high concentration of sulfuric acid was artificially added to the fuel surrogate model to ensure soot activation. The non-volatile particle distribution was based on prior measurements conducted in the PAL using JP-8. The number density of soot particles contained in the sample exhaust was assumed to be 1E12 per cubic meter. A continuous lognormal distribution was prescribed with median diameter of 20-nm and standard deviation of 1.5. This polydisperse distribution was discretized into 24 unique size bins, described in Table 6. The diluent was assumed to be pure nitrogen which enters the probe 2.17E-2-m downstream of the sample inlet. The 1:26 dilution ratio as predicted by the NCC flow solution was also specified in the SGAPE model.

TABLE 6.—INITIAL DISTRIBUTION OF PARTICLE SIZE AND NUMBER DENSITY

Bin Number	Particle Diameter (nm)	Number Density (#/m^3)
1	5.00	1128264111.96
2	6.98	11506806045.05
3	9.75	69465113965.64
4	13.61	213010240128.56
5	19.00	331784413632.47
6	26.52	262502381084.44
7	37.03	105495098724.19
8	51.70	21535407173.25
9	72.18	2233035671.80
10	100.77	117614266.09
11	140.68	3146633.15
12	196.41	42761.60
13	274.22	295.18
14	382.85	1.03
15	534.51	0.00
16	746.25	0.00
17	1041.86	0.00
18	1454.58	0.00
19	2030.79	0.00
20	2835.26	0.00
21	3958.41	0.00
22	5526.48	0.00
23	7715.71	0.00
24	10772.17	0.00

Particle Transport Loss Model Results

Analysis of the non-volatile particle fraction was performed considering changes in the particle size distribution due to diffusion, coagulation, thermophoresis, and nucleation. The flow domain was divided into two segments (see Fig. 11). For segment 1, average pressure, temperature and velocity measurements were extracted from the full CFD solution at 10 axial locations from the probe inlet and supplied as input for the SGAPE model. The axial profile data is listed in Table 7. The predefined exhaust composition was input at the initial station and particle losses by diffusion were tracked at all downstream locations through the end of the segment. Evolution of the particle number for the input particle size distribution is shown in Figure 12. Similarly, segment 2 was divided into 14 axial locations at which the pressure, temperature and velocity were again specified from the CFD solution. All average station values for segment 2 are also listed in Table 7. The output particle size distribution from segment 1 was used as input for segment 2. In addition, a N_2 dilution mass fraction of 26:1 was specified at the first station of segment 2. Evolution of the particle number for segment 2 is shown in Figure 13.

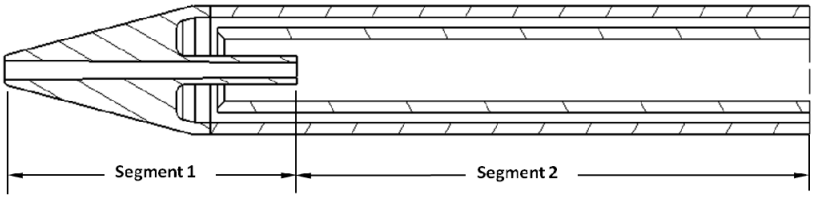

Figure 11.—Division of probe into two segments for analysis of particle transport losses.

TABLE 7.—AVERAGE FLOW FIELD DATA EXTRACTED FROM NCC SOLUTION FOR PROBE SEGMENTS 1 AND 2

Distance From Sample Inlet (m)	Cross Sectional Area (m^2)	Temperature (K)	Pressure (Pa)	Axial Velocity (m/s)
0.00E+00	4.27E-08	235.62	18731.25	10.56
2.29E-03	4.04E-08	235.61	18709.69	11.13
4.57E-03	3.82E-08	235.61	18685.42	11.77
6.86E-03	3.58E-08	235.60	18658.21	12.49
9.14E-03	3.45E-08	235.59	18627.89	13.23
1.14E-02	3.28E-08	235.58	18593.60	14.04
1.37E-02	3.04E-08	235.57	18554.92	14.98
1.60E-02	2.86E-08	235.55	18510.98	16.04
1.83E-02	2.64E-08	235.53	18461.33	17.22
2.06E-02	2.46E-08	235.51	18403.73	18.46
2.17E-02	4.57E-07	285.19	18386.41	33.85
2.40E-02	4.57E-07	287.54	18406.76	33.39
2.63E-02	4.57E-07	289.35	18410.59	33.37
2.86E-02	4.57E-07	290.11	18411.26	33.37
3.09E-02	4.57E-07	290.45	18409.12	33.38
3.31E-02	4.57E-07	290.65	18406.00	33.38
3.54E-02	4.57E-07	290.78	18401.00	33.39
3.77E-02	4.57E-07	290.86	18396.00	33.39
4.00E-02	4.57E-07	290.92	18390.00	33.40
4.23E-02	4.57E-07	290.96	18384.00	33.41
4.46E-02	4.57E-07	290.98	18378.00	33.42
4.69E-02	4.57E-07	290.99	18372.00	33.42
4.92E-02	4.57E-07	290.99	18365.00	33.43
5.14E-02	4.57E-07	290.98	18359.00	33.44

Figure 12 indicates a significant loss in particles through segment 1, which is mostly attributed to diffusion. Because the sample inlet accelerates the incoming fluid stream to better match the velocity of the dilution flow, particle losses of up to 55 percent are realized within the first 2.17E-2-m for all size bins. Despite this large loss, a significant number of particles remain at the sample exit and the overall shape of the particle size distribution remains, for the most part, unchanged. Once dilution flow is added at the start of segment 2, the particle concentration decreases rapidly, but the shape of the size distribution still remains fairly consistent, as evident in Figure 14. Some broadening of the spectrum is also noted, but microphysical effects seem to be significantly reduced by the end of segment 2.

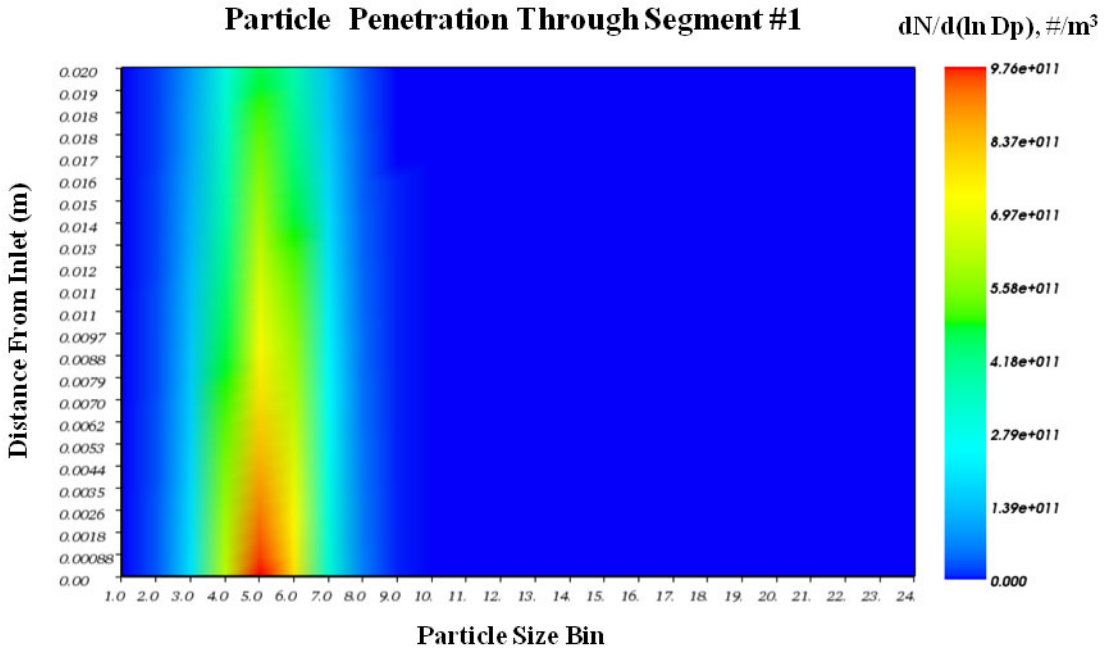

Figure 12.—Particle penetration through segment 1.

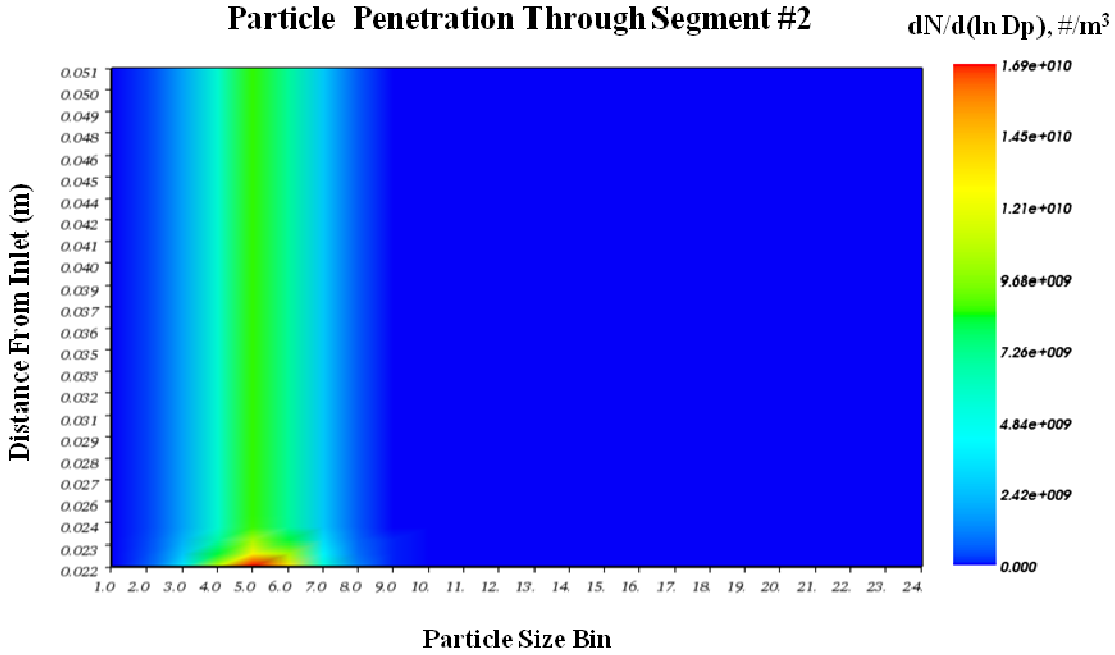

Figure 13.—Particle penetration through segment 2.

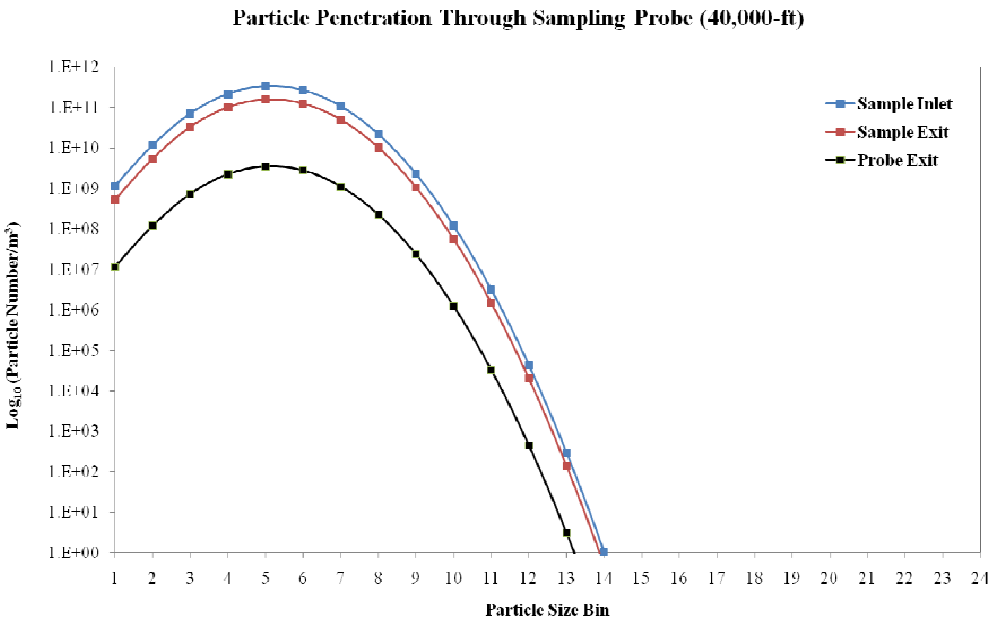

Figure 14.—Evolution of the particle size distribution through the probe entrance region.

Off-Design Performance

Probe off-design performance was analyzed assuming operation at 30,000-ft standard day conditions. A description of the background chamber and sampling probe inlet conditions for this case are provided in Table 8. Burner exhaust conditions were assumed consistent with those from before. The probe geometry and D_{ratio} of 20:1 were maintained for off-design operation. Figure 15 displays the off-design NPSS model block diagram, including input and output flow station parameters. Mach numbers at the dilution and sample exits were allowed to vary to keep the ratio of diluent to sample equal with the on-design case.

TABLE 8(a).—BACKGROUND ALTITUDE CONDITIONS FOR OFF-DESIGN SAMPLING POINT

Altitude Chamber Conditions (30,000-ft)		
U_∞	0.0	m/s
$\rho_{s,\infty}$ @ 30,000-ft std. day	0.458	kg/m^3
$P_{s,\infty}$ @ 30,000-ft std. day	30.089	kPa
$T_{s,\infty}$ @ 30,000-ft std. day	228.71	K

TABLE 8(b).—BURNER EXHAUST CONDITIONS FOR OFF-DESIGN SAMPLING POINT

Sampling Probe Inlet Conditions (30,000-ft)		
x	0.71	m
x_E	0.029	m
d^*	8.265E-3	m
U_x	8.509	m/s
$T_{s,x}$	247.57	K
$P_{s,x}$	30.089	kPa
$\rho_{s,x}$	0.424	kg/m^3

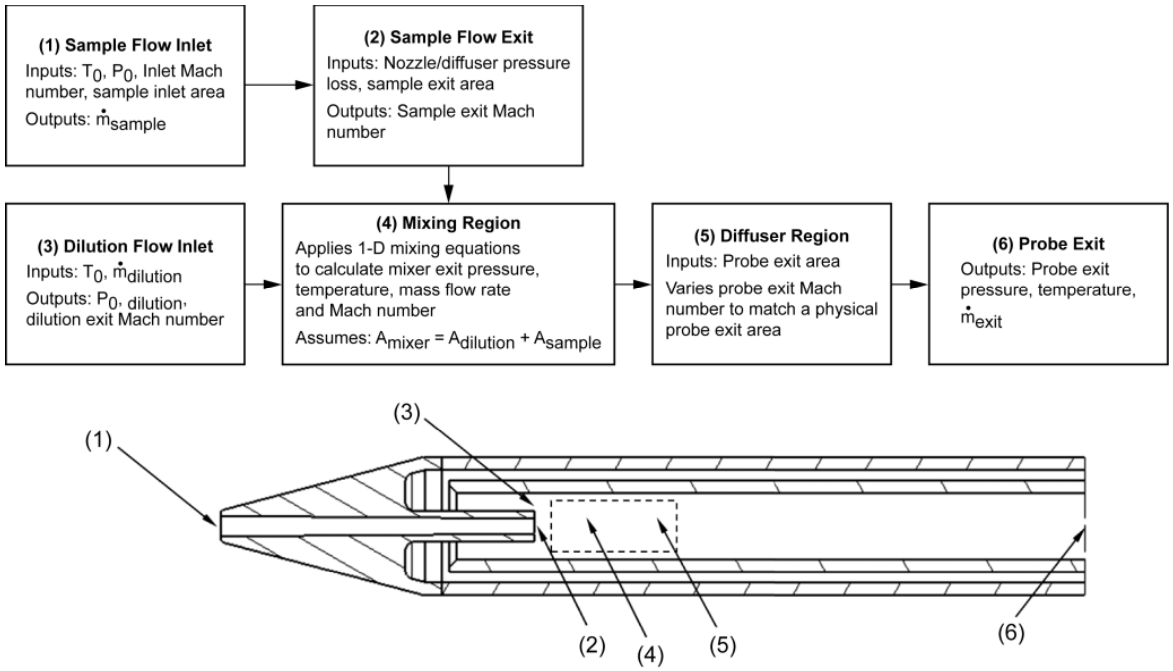

Figure 15.—First-order NPSS model of the high dilution aerosol sampling probe for off-design operation.

TABLE 10.—SAMPLING PROBE DESIGN FROM NPSS MODEL (OFF-DESIGN)

Sample Inlet Flow Station		
Sample Inlet P_s	30.089	kPa
Sample Inlet T_s	247.54	K
Sample Inlet Mach Number	0.028	-
Sample Inlet Mass Flow Rate	5.78E-6	kg/s
Sample Exit Flow Station		
Sample Exit P_s	29.434	kPa
Sample Exit T_s	247.38	K
Sample Exit Mach Number	0.051	-
Dilution Exit Flow Station		
Dilution Exit P_s	29.434	kPa
Dilution Exit T_s	293.67	K
Dilution Exit Mach Number	0.075	-
Dilution Exit Mass Flow Rate	1.16E-4	kg/s
Mixer Exit Flow Station		
Mixer Exit P_s	29.435	kPa
Mixer Exit T_s	291.47	K
Mixer Exit Mach Number	0.073	-
Probe Exit Flow Station		
Probe Exit P_s	29.469	kPa
Probe Exit T_s	291.57	K
Probe Exit Mach Number	0.061	-

The output solution from executing the NPSS model in off-design mode is presented in Table 10.

Computational Fluid Dynamics Results

Similarly to the on-design case, off-design mode operation was analyzed using CFD. Boundary conditions were modified to reflect the values from Tables 8 to 10. Contour plots showing the Mach number, static pressure, static temperature, and mixing fraction for off-design operation are presented in Figures 16 to 19. In general, most flow characteristics compare well with those from the design point. The flow upstream of the probe tip is very close to axial, with an average divergence of 0.14°. Note the fluid velocity entering the probe is reduced compared to the 40,000-ft case to match the slower plume velocity

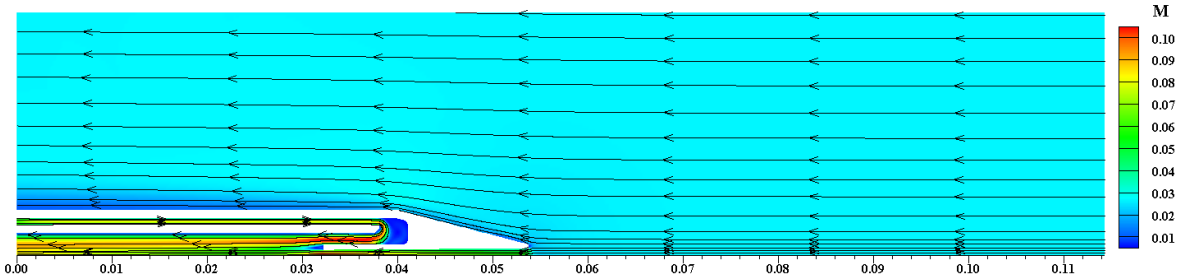

Figure 16.—Vertical plane showing in contour the flow Mach number through the probe inlet with streamlines.

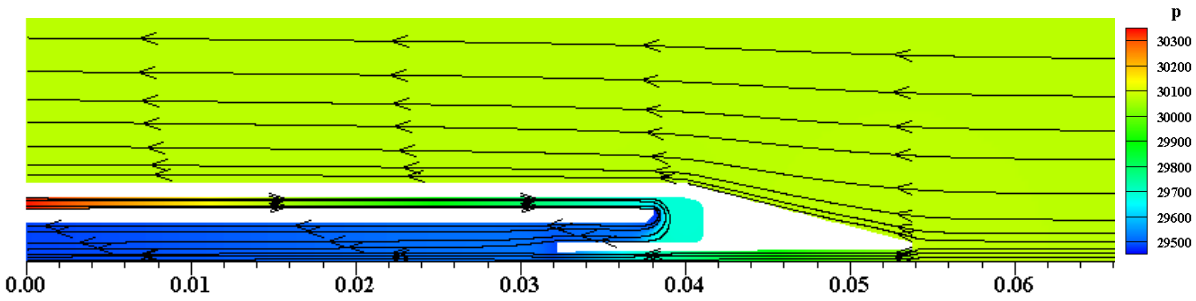

Figure 17.—Vertical plane showing in contour the static pressure through the probe inlet with streamlines.

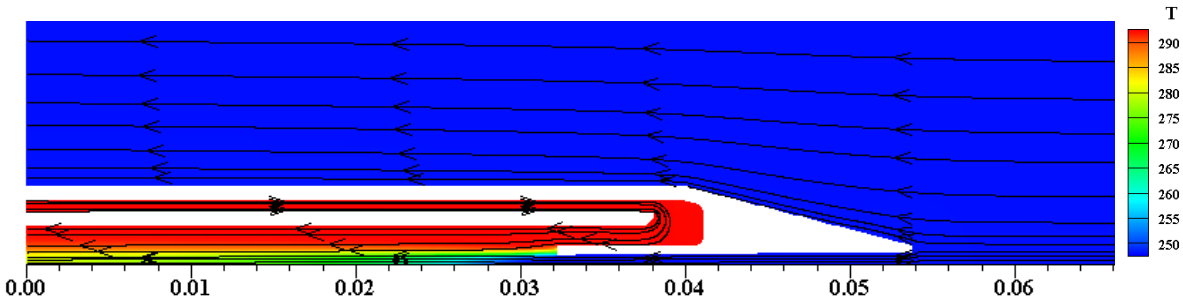

Figure 18.—Vertical plane showing in contour the static temperature through the probe inlet with streamlines.

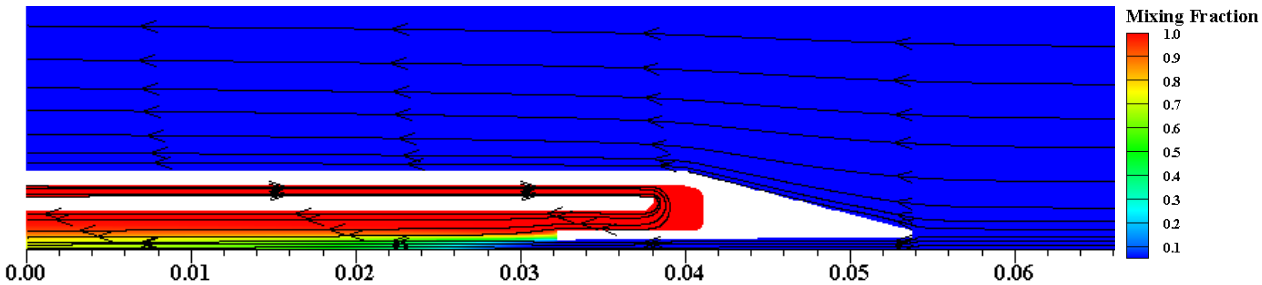

Figure 19.—Vertical plane showing in contour the ratio of dilution to sample with streamlines.

in the chamber. To maintain the same dilution to sample ratio by mass, the mass flow rate of the dilution has also been reduced in the model. The local area Mach numbers for the flow field are typically much lower than for the design case. The most significant difference in off-design operation is that the dilution to sample Mach number ratio has decreased. This allows the incoming sample flow to penetrate further into the dilution stream before mixing occurs. By the exit of the probe segment modeled, the dilution and sample streams have remained separate and are not well-mixed. Additionally, the residence time through the probe has increased allowing chemistry more time to influence the sample distribution. It is expected that the dilution and sample streams would become well-mixed within a relatively short distance beyond the flow domain. More extensive analysis is required to confirm this hypothesis.

For comparison, average flow field values were extracted from the CFD solution at locations representative of the flow stations in the NPSS off-design model. This data is presented in Table 11. For this case, the probe seemed to entrain additional sample flow, causing the sample flow rate from the CFD case to be higher than that predicted by the NPSS model. The D_{ratio} for off-design mode operation from the CFD solution was predicted to be near 13:1.

TABLE 11.—SAMPLING PROBE FLOW STATION PARAMETERS PREDICTED FROM CFD (OFF-DESIGN)

Sample Inlet Flow Station		
Sample Inlet P_s	30.089	kPa
Sample Inlet T_s	247.58	K
Sample Inlet Mach Number	0.045	-
Sample Inlet Mass Flow Rate	9.06E-6	kg/s
Sample Exit Flow Station		
Sample Exit P_s	29.499	kPa
Sample Exit T_s	247.2	K
Sample Exit Mach Number	0.079	-
Dilution Exit Flow Station		
Dilution Exit P_s	29.497	kPa
Dilution Exit T_s	293.4	K
Dilution Exit Mach Number	0.075	-
Dilution Exit Mass Flow Rate	1.16E-4	kg/s
Probe Exit Flow Station		
Probe Exit P_s	29.470	kPa
Probe Exit T_s	291.1	K
Probe Exit Mach Number	0.063	-

Particle Transport Loss Model Results

Similarly to before, the SGAPE tool was applied to the resultant flow solution obtained from NCC. Table 12 gives the average information extracted along the length of the probe and provided as input to the SGAPE code.

TABLE 12.—AVERAGE FLOW FIELD DATA EXTRACTED FROM NCC SOLUTION FOR PROBE SEGMENTS 1 AND 2

Distance From Sample Inlet (m)	Cross Sectional Area (m^2)	Temperature (K)	Pressure (Pa)	Axial Velocity (m/s)
0.00E+00	4.27E-08	247.40	30028.83	14.08
2.29E-03	4.04E-08	247.39	29997.82	14.75
4.57E-03	3.82E-08	247.38	29961.52	15.60
6.86E-03	3.58E-08	247.36	29921.21	16.56
9.14E-03	3.45E-08	247.34	29875.79	17.54
1.14E-02	3.28E-08	247.32	29824.19	18.61
1.37E-02	3.04E-08	247.29	29765.93	19.86
1.60E-02	2.86E-08	247.27	29699.96	21.26
1.83E-02	2.64E-08	247.23	29623.94	22.82
2.06E-02	2.46E-08	247.18	29536.73	24.46
2.17E-02	4.57E-07	288.60	29492.69	21.88
2.40E-02	4.57E-07	289.68	29512.40	21.52
2.63E-02	4.57E-07	290.06	29513.42	21.51
2.86E-02	4.57E-07	290.25	29512.00	21.51
3.09E-02	4.57E-07	290.42	29510.00	21.51
3.31E-02	4.57E-07	290.57	29507.00	21.52
3.54E-02	4.57E-07	290.70	29503.00	21.52
3.77E-02	4.57E-07	290.80	29499.00	21.52
4.00E-02	4.57E-07	290.88	29495.00	21.53
4.23E-02	4.57E-07	290.95	29490.20	21.53
4.46E-02	4.57E-07	291.00	29486.00	21.53
4.69E-02	4.57E-07	291.03	29482.00	21.53
4.92E-02	4.57E-07	291.06	29477.46	21.54
5.14E-02	4.57E-07	291.08	29473.00	21.54

Figures 20 and 21 show the particle penetration through segments 1 and 2 for the off-design case. The general results are nearly identical to those in Figures 12 and 13 for the on-design solution. Particle penetration is slightly better in off-design operation and near 49 percent for all size bins through segment 1. Despite the reduced D_{Ratio} for the off-design case, particle penetration through segment 2 seems to be comparable with the results presented for the on-design simulation.

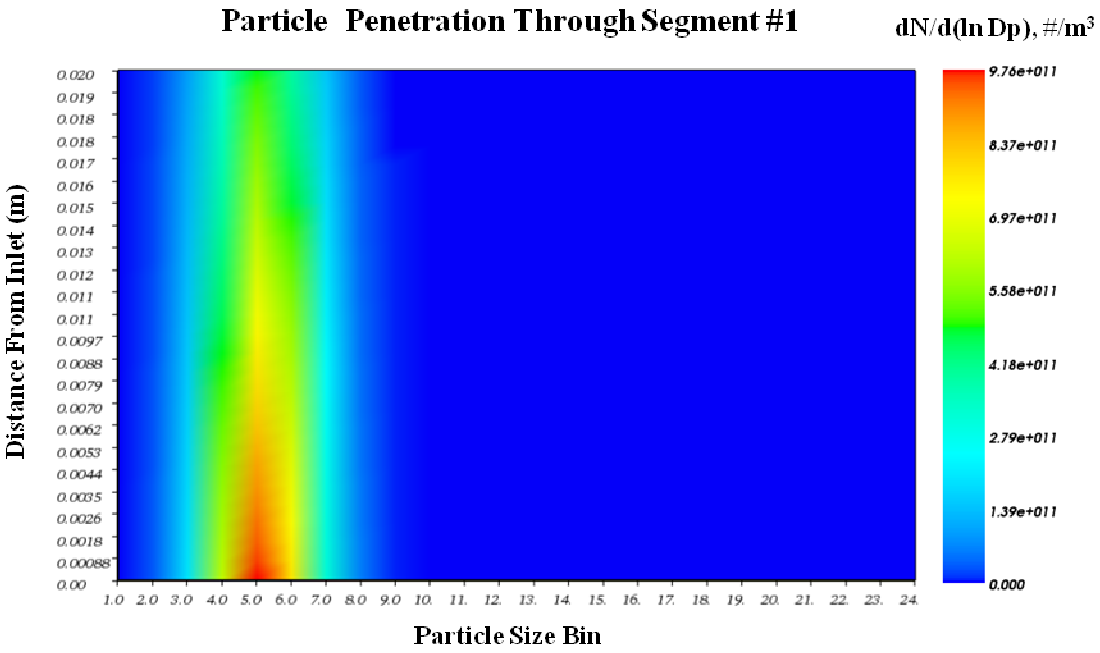

Figure 20.—Particle penetration through segment 1.

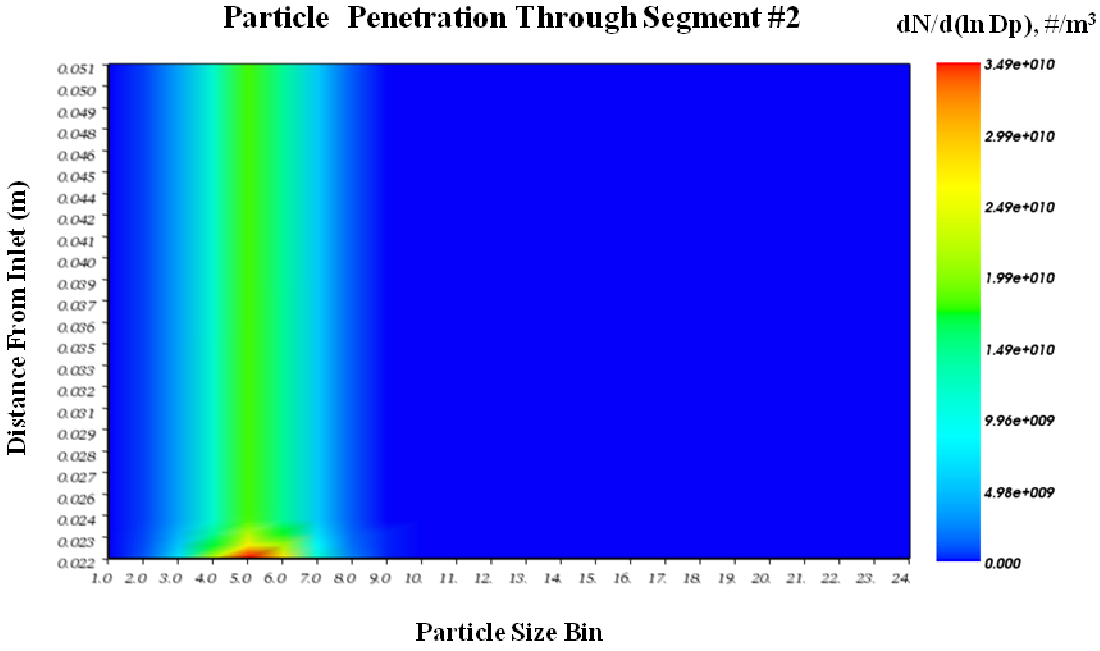

Figure 21.—Particle penetration efficiency through segment 2.

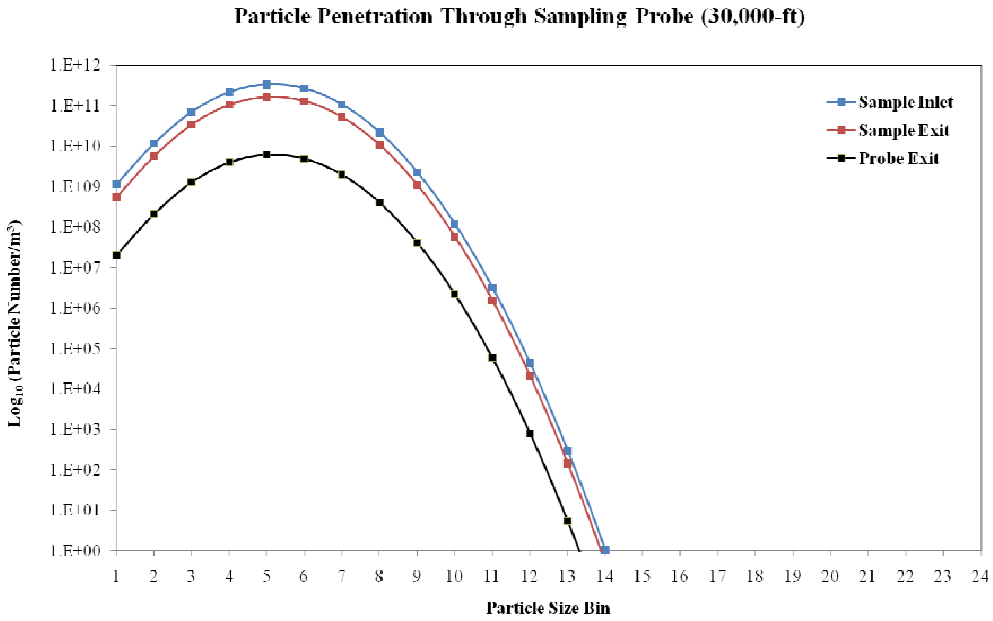

Figure 22.—Evolution of the particle size distribution through the probe entrance region.

Figure 22 shows the particle size distribution at the sample inlet, sample exit, and probe exit for sampling at 30,000-ft conditions. As in the on-design case, some broadening of the initial particle size distribution is evident by the probe exit. Despite this, the overall output distribution is fairly consistent and losses appear to decrease after dilution is added.

An additional factor not considered in this analysis is the effect of an elevated probe wall temperature on particle transport and loss mechanisms. Probe wall temperature can play a significant role in terms of thermophoretic losses. For this study, wall temperature was assumed to be consistent with the temperature of the internal fluid stream, meaning no heating was applied. During sampling, however, exhaust products must be kept warm to reduce the formation of condensates. If the temperature of an extracted sample becomes too high during transport, volatile particles may evaporate, leading to a large reduction in the overall particle number density measured. Further analysis is required to better understand the trade-offs between the volatile and non-volatile particle modes. Once these trade-offs are better characterized, detailed design can be performed to define the best operating practices to measure all submicron particulate matter.

Probe Dimensions

Figure 23 contains drawings of the probe tip design identified and analyzed in this report. As mentioned prior, the probe tip is the primary custom part of this design as it will interface directly with a coaxial pair of thin walled stainless steel tubes.

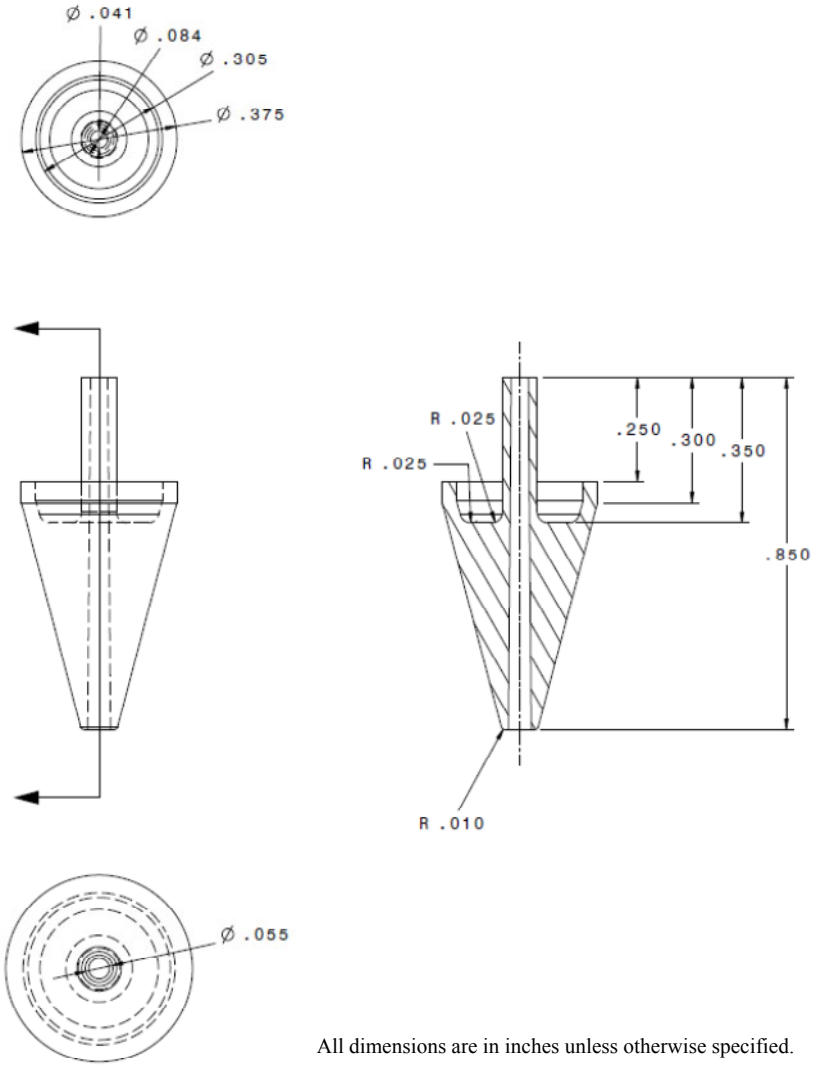

Figure 23.—Dimensions of the final probe tip design, analyzed in on- and off-design modes.

Conclusions

A dilution probe for extracting combustion-generated particles from a high altitude environment has been designed at the preliminary level. The probe operates partially as an eductor/mixer with high velocity dilution flow generating a portion of the vacuum force that draws the sample in through the probe tip. Analysis of the design space was performed using a low-order mixer model developed in the Numerical Propulsion System Simulation (NPSS) code. Detailed analysis was performed by applying computational fluid dynamics to each feasible design output from the NPSS model. Once an acceptable CFD solution was obtained, a data reduction technique was used to extract flow field information along the length of the probe. The average flow field data was supplied as input to a first-order streamline based gas and particle emissions analysis code. A representative soot distribution was prescribed at the inlet of the probe and the particle transport losses due to several common loss mechanisms were estimated along the probe length.

Following the design point analysis, an off-design case was also analyzed. The off-design flow field was found to be acceptable, but mixing rate of the diluent and sample streams was reduced from the on-design case. To match the slower velocity of the jet, the mass flow and Mach number through the off-design probe were reduced. This led to an increase in sampling residence time, which permitted increased chemistry to occur.

Overall, the particle transport model for on- and off-design operation predicted losses near 50 percent for all size bins within the first 2.17E-2-m of the probe entrance. This loss was considered high and thought to be a result of diffusion losses due to the increasing velocity through the sample inlet region. More work may be required to confirm this result and understand why the particle losses through such a short segment are so large. A full CFD solution including an increased reaction mechanism may offer additional insight.

Future Work

This analysis has exposed a series of complications with operating a fixed geometry probe isokinetically in a variety of environments. Careful control of the probe exit pressure is required to ensure that a representative sample is captured from the free stream. When operating with high dilution, the ratio of Mach numbers between the sample and dilution streams must be within a reasonable range to reduce the formation of turbulent eddies inside the probe and upstream of the inlet. Future work is planned to study more advanced probe concepts that include a feedback controller to adjust the sample to dilution mass flow ratio. After further investigation, the final probe design will be manufactured and undergo preliminary testing in the Particle Aerosol Laboratory. Comparison of the predicted performance will be made with the actual performance to validate the success of the design process.

References

1. Tacina, Kathleen M. & Heath, Christopher M., "Evolution of Combustion –Generated Particles at Troposhperic Conditions," Proceedings of the ASME Turbo Expo 2010: Power for Land, Sea and Air, June 4–8, 2010, Glasgow, Scotland.
2. Ram, Michael, Cain, Stuart, & Taulbee, Dale, "Design of a Shrouded Probe For Airborne Aerosol Sampling in a High Velocity Airstream," Journal of Aerosol Science, Volume 26, Issue 6, September 1995, pp. 945–962.
3. Thring, M.W. & Newby, M.P. 1953 Combustion length of enclosed turbulent jet flames. Proc. 4th Intl. Symp. on Combustion, pp. 789–796, Williams & Wilkins, Co., Baltimore.
4. Tacina, Kathleen M. & Dahm, Werner J.A., "Effects of Heat Release on Turbulent Shear Flows. Part 1. A General Equivalence Principle for Non-buoyant Flows and its Application to Turbulent Jet Flames," Journal of Fluid Mechanics, Volume 415, January 2000, pp. 23–44.
5. Stubbs, R., M., and Liu, N.-S., "Preview of the National Combustion Code," AIAA Paper 1997-3114, 33rd AIAA/ASME/SAE/ASEE Joint Propulsion Conference and Exhibit, July 6–9, 1997, Seattle, WA.
6. Chen, K.-H., Norris, A.T., Quealy, A., and Liu, N.-S., "Benchmark Test Cases for The National Combustion Code," 34th AIAA/ASME/SAE/ASEE Joint Propulsion Conference and Exhibit, July 13-15, 1998, Cleveland, OH.
7. Shih, T.-H., Chen, K.-H., and Liu, N.-S., "A Non-Linear k-epsilon Model for Turbulent Shear Flows," AIAA Paper 1998-3983, 1998.
8. Wey, Thomas & Liu, Nan-Suey, "Modeling of Aerosols in Post-Combustor Flow Path and Sampling System," NASA/TM—2006-214397, September 2006.
9. Wey, Thomas & Liu, Nan-Suey, "Streamline-Based Modeling of Aerosol Microphysics in the Post-Combustor Flow Path and Sampling System," AIAA Paper 2007-0794, 45th AIAA Aerospace Sciences, Meeting and Exhibit, January 8-11, 2007, Reno, NV.